LETTER

Asymmetric division of contractile domains couples cell positioning and fate specification

Jean-Léon Maître[1]†, Hervé Turlier[1]*, Rukshala Illukkumbura[1]*, Björn Eismann[1]†, Ritsuya Niwayama[1], François Nédélec[1] & Takashi Hiiragi[1]

During pre-implantation development, the mammalian embryo self-organizes into the blastocyst, which consists of an epithelial layer encapsulating the inner-cell mass (ICM) giving rise to all embryonic tissues[1]. In mice, oriented cell division, apicobasal polarity and actomyosin contractility are thought to contribute to the formation of the ICM[2–5]. However, how these processes work together remains unclear. Here we show that asymmetric segregation of the apical domain generates blastomeres with different contractilities, which triggers their sorting into inner and outer positions. Three-dimensional physical modelling of embryo morphogenesis reveals that cells internalize only when differences in surface contractility exceed a predictable threshold. We validate this prediction using biophysical measurements, and successfully redirect cell sorting within the developing blastocyst using maternal myosin (*Myh9*)-knockout chimaeric embryos. Finally, we find that loss of contractility causes blastomeres to show ICM-like markers, regardless of their position. In particular, contractility controls Yap subcellular localization[6], raising the possibility that mechanosensing occurs during blastocyst lineage specification. We conclude that contractility couples the positioning and fate specification of blastomeres. We propose that this ensures the robust self-organization of blastomeres into the blastocyst, which confers remarkable regulative capacities to mammalian embryos.

During the 8- to 16-cell stage transition, oriented divisions can push one of the daughter cells towards the inside of the embryo[5,7,8]. Alternatively, blastomeres were observed to internalize after the 8- to 16-cell stage division, possibly driven by differences in cell contractility[2,3]. How the embryo generates cell populations with distinct contractile properties is, however, unknown, and the physical mechanism by which this leads to internalization remains disputed[2,3].

We first investigated the origin of the differences in contractility among blastomeres at the 16-cell stage. During the 8-cell stage, blastomeres polarize by forming an apical domain, which occupies only a portion of the contact-free surface. This apical material can be asymmetrically inherited during the following division[2,9], giving rise to both polarized and unpolarized blastomeres within the 16-cell-stage embryo, as can be observed from the levels of the essential apical protein aPKC[4,10,11] (Extended Data Fig. 1). We observe that unpolarized blastomeres, with low levels of aPKC, show higher cortical levels of myosin than polarized ones (Extended Data Fig. 1). Moreover, in embryos knocked out for two isoforms of aPKC[4,10], we observe no reduction of myosin levels where the apical domain would normally be, suggesting that aPKC antagonizes cortical myosin accumulations at the apical domain (Extended Data Fig. 1). As a consequence of reduced levels of myosin, we would expect the apical domain to exhibit reduced contractility. To test this, we took advantage of the periodic contractions that appear during the 8-cell stage[12,13] and used them as a proxy of contractility. Upon polarization of 8-cell-stage blastomeres, we measured

contractions of lower amplitude at the apical domain than in the rest of the cortex (apical/non-apical: $59 \pm 23\%$, mean $\pm$ standard deviation (s.d.), $n = 17$ blastomeres; Fig. 1a–e and Supplementary Video 1). After asymmetric division of 8-cell-stage blastomeres, the polarized 16-cell-stage blastomeres often show no detectable periodicity (52% of 23 polarized blastomeres showing contractions; Fig. 1d and Supplementary Video 2) and their contractions display lower amplitudes than those of unpolarized blastomeres (polarized/unpolarized: $65 \pm 26\%$, mean $\pm$ s.d., $n = 23$ doublets; Fig. 1f–i). More precisely, we find that this difference in contractility between polarized and unpolarized blastomeres intensifies as cells internalize (Extended Data Fig. 2). Contractility in polarized blastomeres remains dampened by the apical domain (Fig. 1j and Extended Data Figs 1–2) and polarized sister cells resulting from symmetric divisions show little cortical heterogeneity and do not internalize (Extended Data Fig. 2). By contrast, unpolarized blastomeres increase their contractility, as initiated during compaction at the 8-cell stage[12], resulting in increasing heterogeneity in doublets stemming from asymmetric divisions (Fig. 1j and Extended Data Fig. 2). In summary, we identify the asymmetric inheritance of the apical domain during the 8- to 16-cell-stage division as the source of differences in contractility among blastomeres.

How these differences in cell contractility physically translate into the internalization of the ICM remains unclear[2,3]. To describe quantitatively the mechanism of internalization, we considered the blastomere surface tensions, which are controlled by actomyosin contractility[14], and used them to build a physical model of blastomere configuration. First, we considered a cell doublet as a minimal system in which one cell envelops its neighbour in an entosis-like process[15] (Extended Data Fig. 2 and Supplementary Video 5). This reductionist approach is justified by the fact that doublets resulting from asymmetrically divided 8-cell-stage blastomeres recapitulate both the morphogenesis and fate specification of the whole embryo[16,17]. Noting γ_c, the surface tension at cell–cell contacts, and γ_i, the tension at the cell–medium interface of the cell i (with $i = 1$ or 2 for a cell doublet; Fig. 2a), we define three dimensionless parameters: a compaction parameter $\alpha = \gamma_c/2\gamma_2$; a volume asymmetry $\beta = (V_1/V_2)^{1/3}$, where V_1 and V_2 are the volumes of each cell; and a tension asymmetry $\delta = \gamma_1/\gamma_2$. We can analytically derive the conditions for cell internalization (Fig. 2b, c, Supplementary Video 3 and Supplementary Note). Full internalization occurs whenever $\delta > 1 + 2\alpha$ (Fig. 2b, c), thus defining an internalization threshold $\delta_c = 1 + 2\alpha$ for the tension asymmetry, in agreement with previous numerical studies[18–20]. Before this transition, partial internalization configurations are predicted, which match the configurations observed experimentally in doublets of 16-cell-stage blastomeres (Extended Data Fig. 2 and Supplementary Video 5). Interestingly, the internalization threshold δ_c is not influenced by the size asymmetry β but depends critically on the compaction parameter α (Extended Data Fig. 3). Modulating α in the absence of tension asymmetry is, however, not sufficient for driving
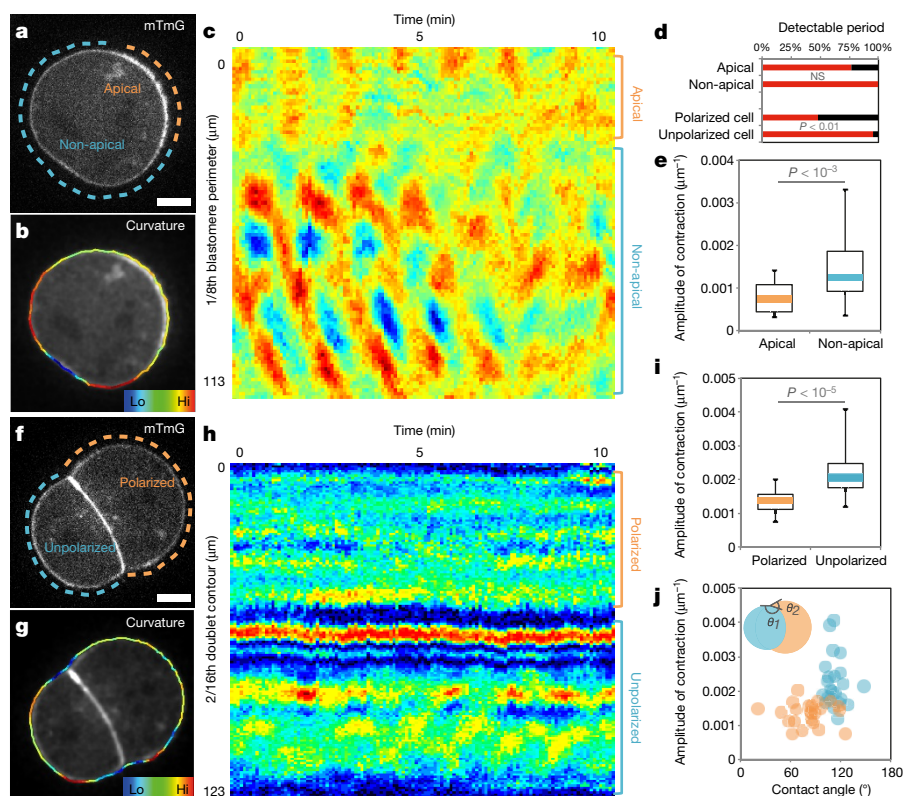
Figure 1 | Asymmetric inheritance of the apical domain generates blastomeres of different contractility. a–c, Eight-cell-stage blastomere expressing mTmG (**a**) with colour-coded surface curvature (**b**) and corresponding kymograph (**c**). Apical domain is highlighted in orange and non-apical cortex in blue. **d**, Proportion of blastomeres for which a contraction period can be detected (17 blastomeres and 23 doublets from 4 and 5 experiments, respectively). Mann–Whitney U-test P value; NS, not significant. **e**, Box plot of contraction amplitudes for apical (orange) and non-apical cortex (blue). Seventeen blastomeres from four experiments, Student's t-test P value. **f–h**, Doublet of 16-cell-stage blastomeres expressing mTmG (**f**) with colour-coded surface curvature (**g**) and corresponding kymograph (**h**). Polarized blastomere is highlighted in orange, unpolarized one in blue. **i**, Box plot of contraction amplitudes for polarized (orange) and unpolarized blastomeres (blue). Twenty-three doublets from four experiments. Student's t-test P value. **j**, Amplitude of contractions as a function of the contact angles θ_1 for polarized (orange) and θ_2 for unpolarized blastomeres (blue, Pearson $R = -0.611$, $n = 46$ blastomeres from five experiments, $P < 0.001$). Scale bars, 10 μm.
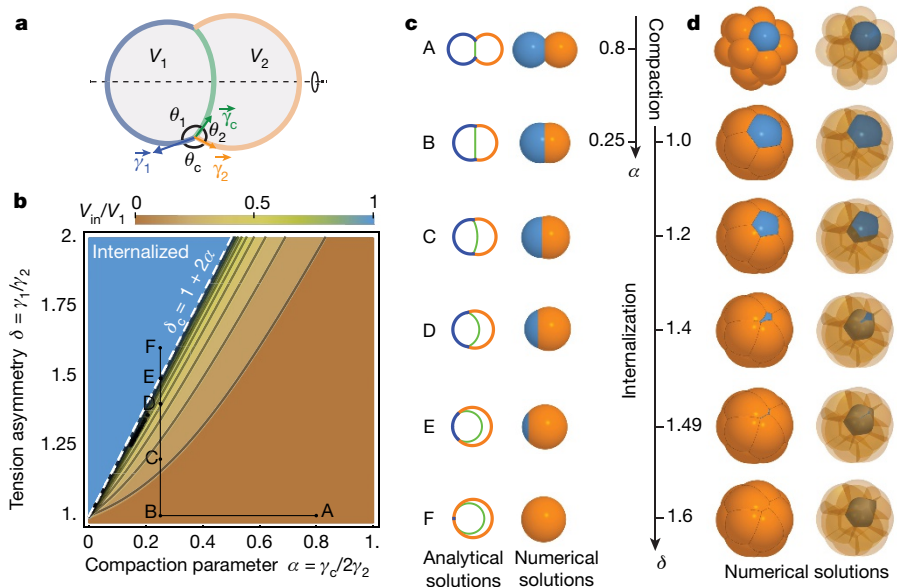

Figure 2 | Physical model of cell internalization. a, Schematic diagram of a cell doublet with surface tensions γ_1, γ_2 and γ_c of cell 1 (blue), 2 (orange) and the contact (green), respectively. Contact angles θ_1, θ_2 and θ_c and cell volumes V_1 and V_2 are also shown. **b**, Phase diagram describing the mechanical equilibrium of a doublet as a function of the compaction parameter α and tension asymmetry δ. Colour-coded degree of internalization (measured as the relative volume of cell 1 that is internalized

V_{in}/V_1), threshold value δ_c at which internalization occurs (white dotted line) and an example of compaction (A to B) followed by internalization (B to F) in black (Supplementary Video 3–4) are overlaid. **c–d**, Analytical (left) and numerical solutions (right) for a doublet (**c**). Numerical solutions (**d**) for the compaction of 16 cells with opaque (left) and transparent (right) non-internalizing cells. The compaction parameter α decreases from 0.8 to 0.25, followed by an increase of tension asymmetry δ from 1.0 to 1.6.
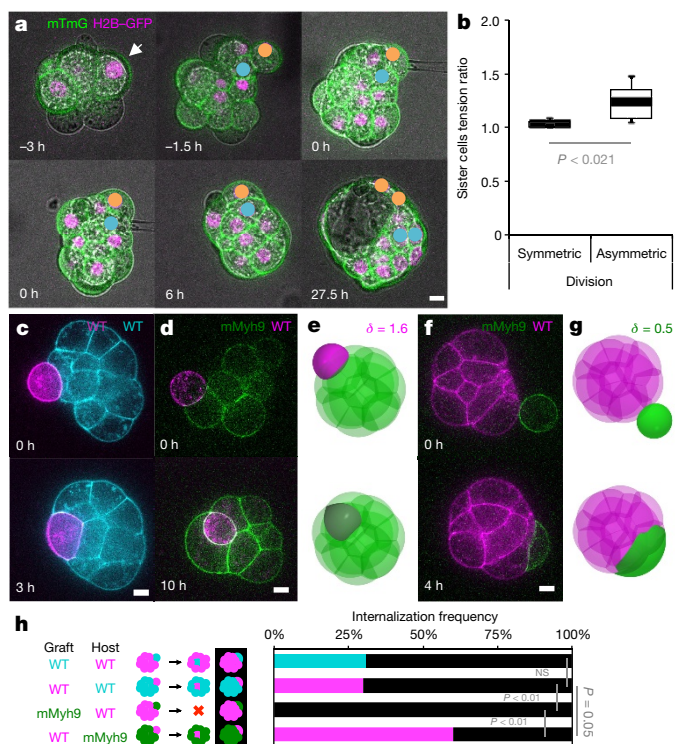
Figure 3 | Tension heterogeneities drive cell sorting of the ICM.
a, Lineage tracking of polarized (yellow) and unpolarized (blue) daughter cells after surface tension measurement of mTmG (green) and H2B–GFP (magenta) expressing embryos. **b**, Box plot of surface tension ratio for sister cells with (symmetric) or without (asymmetric) internalization of one of the sister cell. Eight and seven pairs of cells from eleven embryos from five experiments, Student's t-test P values. **c–g**, Wild-type (WT; magenta or cyan) or mMyh9 (green) blastomeres grafted onto host embryos (**c**, **d**, **f**). Simulations of grafting experiments: one cell with $\delta = 1.6$ (**e**), corresponding to wild type onto mMyh9 (**d**); one cell with $\delta = 0.5$ (**g**), corresponding to mMyh9 onto wild type (**f**). **h**, Internalization frequencies for chimaeric embryos (wild type–wild type (13 mG host embryos and 20 mTmG host embryos from 3 experiments) and wild type–mMyh9 (12 mG host embryos and 20 mMyh9 host embryos from 4 experiments)). Black indicates that no internalization occurs, Mann–Whitney U-test P values; NS, not significant. Scale bars, 10 μm.

internalization. For the value of the compaction parameter measured at late 8-cell stage[12], $\alpha \approx 0.25$, we predict that any tension asymmetry δ higher than $\delta_c \approx 1.5$ should lead to complete internalization (Fig. 2b, c). Therefore, when measuring tension asymmetries, we expect that δ should not exceed ~1.5, otherwise the cell should be fully internalized and hence inaccessible to non-invasive methods.

To generalize this approach to the formation of the ICM in an embryo with 16 cells, we built a three-dimensional numerical model of the embryo using a multi-material mesh-based surface-tracking method[21] (Supplementary Note). We find in simulated embryos the same internalization conditions as in cell doublets, with a transition occurring above the threshold value $\delta_c \approx 1.5$ (Fig. 2d, Extended Data Fig. 7 and Supplementary Video 4). Therefore, the same physical mechanisms can explain the envelopment of one cell by another[15] and the sorting of cells within a tissue[18,19,22,23].

To test the predictions of the model experimentally, we used microaspiration to measure the surface tensions of sister cells after the 8- to 16-cell-stage division, visualize their internalization and then track their position within the blastocyst (Fig. 3a and Supplementary Video 6). Sister cells remaining at the surface of the embryo and failing to contribute to the ICM in the blastocyst show no tension asymmetry at the 16-cell stage ($\delta = 1.04 \pm 0.03$, mean ± s.d., $n = 8$ pairs of sister cells; Fig. 3b). On the other hand, when one sister cell internalizes after the 8- to

16-cell-stage division and contributes to the ICM within the blastocyst, we measure a tension asymmetry of 1.24 ± 0.17 (mean ± s.d., $n = 7$ pairs of sister cells; Fig. 3b). This confirms that asymmetric divisions are the source of tension heterogeneities in the embryo. Furthermore, the observation that internalizing cells are the only ones showing tension heterogeneity relative to their sister cells supports the hypothesis that tension heterogeneity is sufficient to drive cell internalization. Finally, the measured tension asymmetries are indeed lower than the internalization threshold value $\delta_c \approx 1.5$, as predicted by our theory.

To test directly the proposed internalization mechanism, we first generated embryos that lack the maternal allele of *Myh9* (ref. 24; mMyh9 hereafter), the specific isoform of myosin heavy chain that is required for pre-implantation development (zygotic[25] and maternal zygotic Myh10-knockout embryos form normal blastocysts; Supplementary Video 7). Although compaction is delayed due to their inability to generate sufficient tensions[12] (Extended Data Fig. 4), these embryos form blastocysts (Supplementary Video 8) and viable offspring. Next, we transplanted onto a mMyh9 host embryo a wild-type blastomere, which typically internalizes (60% of 20 grafted blastomeres internalized; Fig. 3d, h and Supplementary Video 9; for corresponding numerical simulation, see Fig. 3e and Supplementary Video 10) and contributes to the ICM of the host embryo. By contrast, when transplanted onto wild-type embryos, an mMyh9 blastomere always remains at the surface of the embryo (none of 12 grafted blastomeres internalized; Fig. 3e, h and Supplementary Video 11; for corresponding numerical simulation, see Fig. 3g and Supplementary Video 12), and stretches to envelop blastomeres of the host embryo. In comparison, transplanting wild-type cells onto wild-type hosts leads to a lower internalization frequency than with mMyh9 hosts (31% of 33 blastomeres internalized, $P = 0.05$; Fig. 3c, h and Supplementary Video 13). We conclude that the hierarchy of contractility between blastomeres is sufficient to direct cell internalization. As internalizing cells do not have an apical domain (Fig. 1 and Extended Data Figs 1–2) and do not require intact contractility of neighbouring cells (Fig. 3d), the mechanism by which cells internalize is analogous to a cell sorting process[22] and is distinct from an apical constriction, as previously proposed[3].

While cells adopt their position within the embryo, they segregate into two distinct lineages: trophectoderm and ICM. In the mouse embryo, this lineage specification is regulated by Yap subcellular localization[4,11], which, in cultured cells, is regulated by contractile forces[6]. Therefore, we tested whether contractility influences Yap localization and thereby fate specification. In agreement with previous studies[2,4], we find less cytoplasmic phosphorylated Yap in cells closer to the surface than in the internalized ones (Extended Data Fig. 5a, h). These blastomeres initiate trophectoderm specification as their surface cells show the highest Cdx2 levels (Extended Data Fig. 5a, o). In embryos treated with different concentrations of the myosin inhibitor blebbistatin (Bb), the correlation between these fate markers and cell position is weakened in a dose-dependent manner (Extended Data Figs 5–6). Moreover, mMyh9 embryos show similar defects at the 16-cell stage (Extended Data Figs 5g, n, u and 6c, f), despite being viable (unlike Bb-treated embryos). While inhibiting contractility de-compacts embryos[12], the position of cells is not shuffled, and yet the localization of Yap is affected. During cell internalization, outer cells deform extensively. This is especially the case for doublets in which, similarly to complete embryos, cytoplasmic localization of phosphorylated Yap is lowest for outer cells (Fig. 4a, c, d). When cell deformation is blocked by Bb treatment, phosphorylated Yap localization and Cdx2 levels become homogeneous within doublets (Fig. 4b–f). Remarkably, inhibition of contractility causes both blastomeres to become inner-cell-like with respect to phosphorylated Yap localization and Cdx2 levels, despite their external position (Fig. 4). This is consistent with internalizing cells reducing their contractility over their entire surface, since cell–cell contacts have a contractility equivalent to Bb-treated cells[12]. Together, these results indicate that without contractile forces, blastomeres adopt an inner-cell-like fate,
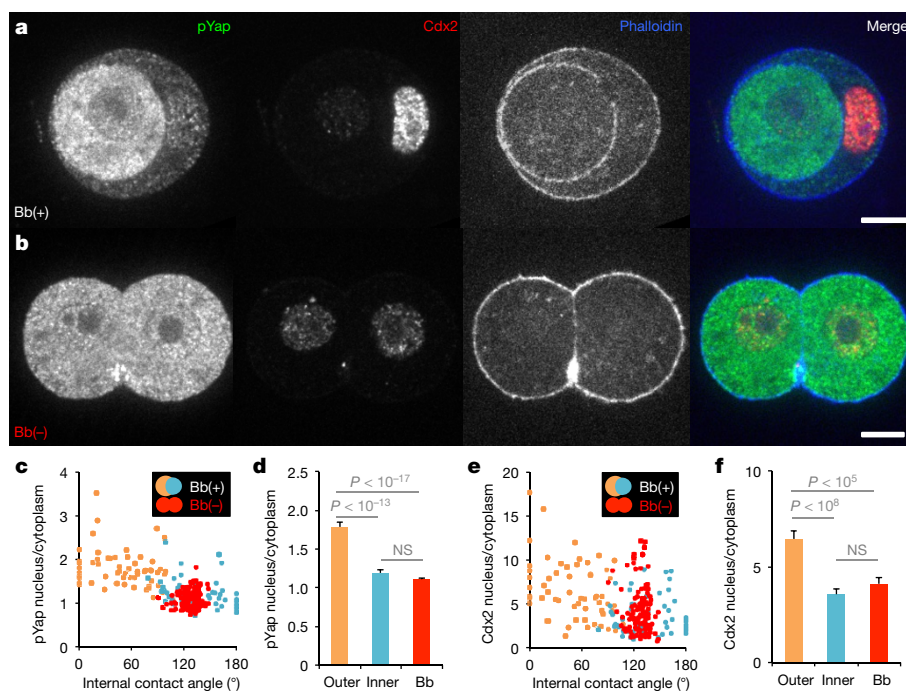
Figure 4 | Contractility couples morphogenesis and fate specification.
a, **b**, Immunostaining of doublets of 16-cell-stage blastomeres treated with 25 μM Bb(+) (**a**; an inactive enantiomere of the inhibitor) or Bb(−) (**b**; the selective inhibitor of myosin II ATPase activity) showing phosphorylated (p)Yap (green), Cdx2 (red) and phalloidin (blue). **c**–**f**, Nucleus-to-cytoplasm intensity ratio of pYap (**c**) or Cdx2 (**e**) as a function of the internal contact angle for doublets treated with Bb(+)

(outer cells in orange and inner cells in blue, pYap $R = -0.630$, or Cdx2 $R = -0.493$, $n = 59$ doublets from 3 experiments, $P < 0.001$) or Bb(−) (red, pYap $R = 0.158$, or Cdx2 $R = -0.118$, $n = 60$ doublets from 3 experiments, $P > 0.1$). Mean ± standard error of the mean (s.e.m.) nucleus to cytoplasm intensity ratio of pYap (**d**) or Cdx2 (**f**). For doublets treated with Bb(+), outer cells are shown in orange and inner cells in blue, while Bb(−)-treated cells are in red. Student's *t*-test *P* values; NS, not significant.

regardless of their position. Therefore, disrupting contractility uncouples morphogenesis and fate specification. Moreover, the control of Yap subcellular localization by contractile forces, reminiscent of those from cell culture studies[6], raises the possibility that lineage specification in the blastocyst could be mechanosensitive. Whether cells may sense their macroscopic deformation[26] or stresses at the molecular level[27], will require further studies. Such mechanosensitivity could explain why inner-cell-like localization of Yap is often observed for blastomeres before they have completed their internalization[2,4] (Extended Data Figs 5–6). We propose that the coupling of cell positioning and fate specification by contractility enables blastomeres to anticipate their final position and initiate their differentiation accordingly.

Apicobasal polarity can control the position of blastomeres by orienting the 8- to 16-cell-stage divisions relative to the surface of the embryo[5]. However, oriented cell divisions do not guarantee that internalized cells will be maintained inside the embryo. We find that apicobasal polarity also controls internalization by maintaining low contractility at the apical domain (Fig. 1). This allows unpolarized blastomeres to outcompete their polarized neighbours when their contractility grows above a threshold value (Figs 2 and 3). The resulting cell sorting is a fail-safe mechanism to one-shot oriented cell divisions. Such complementary mechanisms, together with the ability of cells to read mechanical cues[6] to guide their differentiation[28] (Fig. 4), can account for the regulative capacity of early mammalian embryos[7]. From this study, a self-organization framework determining the initial steps of morphogenesis and lineage specification in mammalian embryos is emerging.

Online Content Methods, along with any additional Extended Data display items and Source Data, are available in the online version of the paper; references unique to these sections appear only in the online paper.

1. Wennekamp, S., Mesecke, S., Nédélec, F. & Hiiragi, T. A self-organization framework for symmetry breaking in the mammalian embryo. *Nature Rev. Mol. Cell Biol.* **14,** 452–459 (2013).
2. Anani, S., Bhat, S., Honma-Yamanaka, N., Krawchuk, D. & Yamanaka, Y. Initiation of Hippo signaling is linked to polarity rather than to cell position in the pre-implantation mouse embryo. *Development* **141,** 2813–2824 (2014).
3. Samarage, C. R. *et al.* Cortical tension allocates the first inner cells of the mammalian embryo. *Dev. Cell* **34,** 435–447 (2015).
4. Hirate, Y. *et al.* Polarity-dependent distribution of angiomotin localizes Hippo signaling in preimplantation embryos. *Curr. Biol.* **23,** 1181–1194 (2013).
5. Dard, N., Louvet-Vallée, S. & Maro, B. Orientation of mitotic spindles during the 8- to 16-cell stage transition in mouse embryos. *PLoS ONE* **4,** e8171 (2009).
6. Dupont, S. *et al.* Role of YAP/TAZ in mechanotransduction. *Nature* **474,** 179–183 (2011).
7. Johnson, M. H. From mouse egg to mouse embryo: polarities, axes, and tissues. *Annu. Rev. Cell Dev. Biol.* **25,** 483–512 (2009).
8. Watanabe, T., Biggins, J. S., Tannan, N. B. & Srinivas, S. Limited predictive value of blastomere angle of division in trophectoderm and inner cell mass specification. *Development* **141,** 2279–2288 (2014).
9. Johnson, M. H. & Ziomek, C. A. The foundation of two distinct cell lineages within the mouse morula. *Cell* **24,** 71–80 (1981).
10. Matsumoto, M. *et al.* PKCλ in liver mediates insulin-induced SREBP-1c expression and determines both hepatic lipid content and overall insulin sensitivity. *J. Clin. Invest.* **112,** 935–944 (2003).
11. Hirate, Y. *et al.* Par-aPKC-dependent and -independent mechanisms cooperatively control cell polarity, Hippo signaling, and cell positioning in 16-cell stage mouse embryos. *Dev. Growth Differ.* **57,** 544–556 (2015).
12. Maître, J.-L., Niwayama, R., Turlier, H., Nédélec, F. & Hiiragi, T. Pulsatile cell-autonomous contractility drives compaction in the mouse embryo. *Nature Cell Biol.* **17,** 849–855 (2015).
13. Lehtonen, E. Changes in cell dimensions and intercellular contacts during cleavage-stage cell cycles in mouse embryonic cells. *J. Embryol. Exp. Morphol.* **58,** 231–249 (1980).
14. Heisenberg, C.-P. & Bellaïche, Y. Forces in tissue morphogenesis and patterning. *Cell* **153,** 948–962 (2013).
15. Overholtzer, M. *et al.* A nonapoptotic cell death process, entosis, that occurs by cell-in-cell invasion. *Cell* **131,** 966–979 (2007).
16. Dietrich, J.-E. & Hiiragi, T. Stochastic patterning in the mouse pre-implantation embryo. *Development* **134,** 4219–4231 (2007).
17. Johnson, M. H. & Ziomek, C. A. Cell interactions influence the fate of mouse blastomeres undergoing the transition from the 16- to the 32-cell stage. *Dev. Biol.* **95,** 211–218 (1983).

18. Graner, F. & Glazier, J. A. Simulation of biological cell sorting using a two-dimensional extended Potts model. *Phys. Rev. Lett.* **69**, 2013–2016 (1992).

19. Brodland, G. W. The Differential Interfacial Tension Hypothesis (DITH): a comprehensive theory for the self-rearrangement of embryonic cells and tissues. *J. Biomech. Eng.* **124**, 188–197 (2002).

20. Guzowski, J., Korczyk, P. M., Jakiela, S. & Garstecki, P. The structure and stability of multiple micro-droplets. *Soft Matter* **8**, 7269–7278 (2012).

21. Da, F., Batty, C. & Grinspun, E. Multimaterial mesh-based surface tracking. *ACM Trans. Graph.* **33**, 112 (2014).

22. Krieg, M. *et al.* Tensile forces govern germ-layer organization in zebrafish. *Nature Cell Biol.* **10**, 429–436 (2008).

23. Maître, J.-L. *et al.* Adhesion functions in cell sorting by mechanically coupling the cortices of adhering cells. *Science* **338**, 253–256 (2012).

24. Jacobelli, J. *et al.* Confinement-optimized three-dimensional T cell amoeboid motility is modulated via myosin IIA-regulated adhesions. *Nature Immunol.* **11**, 953–961 (2010).

25. Wang, A. *et al.* Nonmuscle myosin II isoform and domain specificity during early mouse development. *Proc. Natl Acad. Sci. USA* **107**, 14645–14650 (2010).

26. Aragona, M. *et al.* A mechanical checkpoint controls multicellular growth through YAP/TAZ regulation by actin-processing factors. *Cell* **154**, 1047–1059 (2013).

27. Benham-Pyle, B. W., Pruitt, B. L. & Nelson, W. J. Mechanical strain induces E-cadherin-dependent Yap1 and β-catenin activation to drive cell cycle entry. *Science* **348**, 1024–1027 (2015).

28. Shin, J.-W. *et al.* Contractile forces sustain and polarize hematopoiesis from stem and progenitor cells. *Cell Stem Cell* **14**, 81–93 (2014).

METHODS

Embryo work. *Recovery and culture.* All animal work was performed in the animal facility at the European Molecular Biology Laboratory, with permission from the institutional veterinarian overseeing the operation (ARC number TH11 00 11). The animal facilities are operated according to international animal welfare rules (Federation for Laboratory Animal Science Associations guidelines and recommendations).

Embryos are isolated from superovulated female mice mated with male mice. Superovulation of female mice is induced by intraperitoneal injection of 5 international units (IU) of pregnant mare's serum gonadotropin (PMSG; Intervet Intergonan), followed by intraperitoneal injection of 5 IU human chorionic gonadotropin (hCG; Intervet Ovogest 1500) 44–48 h later. Two-cell-stage (embryonic day 1.5 (E1.5)) embryos are recovered by flushing oviducts from plugged females with 37 °C FHM (Millipore, MR-024-D) using a custom-made syringe (Acufirm, 1400 LL 23).

Embryos are handled using an aspirator tube (Sigma, A5177-5EA) equipped with a glass pipette pulled from glass micropipettes (Blaubrand intraMark).

Embryos are placed in KSOM (Millipore, MR-121-D) or FHM supplemented with 0.1% BSA (Sigma, A3311) in 10 μl droplets covered in mineral oil (Sigma, M8410 or Acros Organics). Embryos are cultured in an incubator with a humidified atmosphere supplemented with 5% CO_2 at 37 °C.

For imaging, embryos are placed in 5 cm glass-bottom dishes (MatTek).

Mouse lines. (C57BL/6xC3H) F1 hybrid strain is used for wild type (WT).

To visualize filamentous actin, LifeAct–GFP mice (*Tg(CAG-EGFP)#Rows*) are used[29]. To visualize plasma membranes, mTmG mice (*Gt(ROSA) 26Sor^tm4(ACTB-tdTomato,-EGFP)Luo*) are used[30]. To visualize nuclei, H2B–GFP mice are used[31]. Genes are deleted maternally using Zp3-cre (*Tg(Zp3-cre)93Knw*) mice[32]. To generate mMyh9 embryos, *Myh9^tm5RSad* mice are used[24] to breed *Myh9^tm5RSad/tm5RSad*; *Zp3^Cre/+* mothers with WT fathers. To generate mzMyh10 embryos, *Myh10^tm7Rsad* mice were used[33] to breed *Myh10^tm7Rsad/tm7Rsad*; *Zp3^Cre/+* mothers with *Myh10^+/−* fathers. To generate aPKC-knockout embryos, *Prkci^tm1Kido* (ref. 10) and *Prkcz^tm1.1Cda* (ref. 4) mice are used to breed *Prkci^−/−*; *Prkcz^+/−* fathers with *Prkci^−/−*; *Prkcz^tm1.1Cda/+*; *Zp3^Cre/+* mothers.

Mice were used from 6 weeks old onwards.

Chemical reagents. Blebbistatin(+), an inactive enantiomere of the inhibitor, or (−), the selective inhibitor of myosin II ATPase activity (Tocris, 1853 and 1852), and 50 mM DMSO stocks are diluted to 5, 12.5 or 25 μM in KSOM.

Isolation of blastomeres at the 8- and 16-cell stage. Embryos are dissected out of their zona pellucida (ZP) at the 2- to 4-cells stage. ZP-free 8- or 16-cell stage embryos are placed into Ca^{2+}-free KSOM for 5–10 min before being aspirated multiple times (typically between 3 and 5 times) through a narrow glass pipette (with a radius between that of an 8- or 16-cell-stage blastomere and of the whole embryo) until dissociation of cells. To form doublets of polarized and unpolarized 16-cell-stage blastomeres, an 8-cell-stage blastomere is cultured until asymmetric division. To form chimaeras, 16-cell-stage blastomeres are grafted onto a complete embryo using a mouth pipette.

Immunostaining. Primary antibody targeting the double phosphorylated form (Thr18/Ser19) of the myosin regulatory light-chain (Cell Signaling, 3674), PKC-ζ (Santa Cruz, sc-17781), Yap (Abnova, M01, clone 2F12) or its Ser127 phosphorylated form (Cell Signaling, 4911) are used at 1:100. The primary antibody targeting Cdx2 (Biogenex, MU392A-UC) or phosphorylated form (Ser1943) of the non-muscle myosin heavy chain Myh9 (Cell Signaling, 5026) are used at 1:200.

Secondary antibody targeting mouse or rabbit IgG coupled to Alexa Fluor 488 or 546 (Life Technologies) are used at 1:250. Alexa Fluor 633-coupled (ThermoFisher, A22284) phalloidin is used at 1:250.

Micropipette aspiration. As described previously[12], a microforged micropipette coupled to a microfluidic pump (Fluigent, MFCS) is used to measure the surface tension of cells. In brief, micropipettes of radii 7–8 μm for 8-cell-stage embryos and 2.5–3.5 μm for 16-cell-stage embryos are used to apply step-wise increasing pressures on blastomeres until reaching a deformation which has the radius of the micropipette (R_p). At steady state, the surface tension γ_1 of the blastomere is calculated based on Young–Laplace's law: $\gamma_1 = P_c/2(1/R_p - 1/R_c)$, where P_c is the pressure used to deform the cell of radius R_c.

Asymmetric division tracing. To measure the tension of sister cells at the 16-cell stage, time-lapse images of mTmG and H2B–GFP expressing embryos were taken every 30 min from the 8-cell stage onwards. The 8- to 16-cell-stage divisions are tracked, the time lapse is paused to measure the surface tension of both sister cells. After resuming the time lapse, the measured cells are tracked until blastocyst stage.

When both sister cells remain at the surface of the embryo, the division is considered symmetric, whereas when one sister cell internalizes during the 16-cell stage and becomes part of the ICM, the division is considered asymmetric.

Microscopy. Tension measurements are performed on a Zeiss Axio Observer microscope with a dry × 20/0.8 PL Apo DICII objective. The microscope is equipped with an incubation chamber to keep the sample at 37 °C. Tension measurements and confocal images are taken using an inverted Zeiss Observer Z1 microscope with a CSU-X1M 5000 spinning disc unit. Excitation is achieved using 488 nm, 561 nm and 633 nm laser lines through a × 63/1.2 C Apo W DIC III water immersion objective. Emission is collected through 525/50 nm, 605/40 nm, 629/62 nm band pass or 640 nm low pass filters onto an EMCCD Evolve 512 camera. The microscope is equipped with an incubation chamber to keep the sample at 37 °C and supply the atmosphere with 5% CO_2.

Data analysis. *Shape analysis.* Using FIJI, we manually fit a circle onto the cell-medium interface to measure the radius of curvature of the cell R_c. We use the angle tool to measure the contact angles θ_1, θ_2 and θ_c. We draw a line perpendicular to the micropipette tip and use the linescan function to measure the diameter of the micropipette and calculate R_p.

Intensity ratio measurements. Using FIJI, we pick confocal slices cutting through the equatorial plane of the apical domain or of two contacting cells. We draw a ~1 μm thick line along the cell-medium interface of the apical and non-apical regions or of each cell and measure the mean intensity. The apical region is defined by visually observing aPKC or mTmG enrichment in the central region of the cell-medium interface. For aPKC-knockout embryos, the actin-rich region at the centre of the cell-medium interface is selected. The transition zones between apical and non-apical or close to cell–cell contacts between polarized and unpolarized cells are excluded to calculate intensity ratios (~5 μm).

Using FIJI, we pick confocal slices cutting through the equatorial plane of the nucleus of a cell. We draw a 2.5 μm radius circle and measure the average intensity in the nucleus and, next to it, in the cytoplasm. We then calculate the nucleus-to-cytoplasm intensity ratio. For whole embryos, the closest distance of the nucleus to the surface of the embryo, marked by phalloidin staining, is measured using the line tool.

Periodic contractions analysis. To analyse periodic contractions, we used a previously described pipeline[12]. In brief, mTmG images are used to segments the cells outlines into 100 equidistant nodes for 8-cell-stage blastomeres and 150 for 16-cell-stage blastomeres doublets. From those nodes, three nodes spaced by 10 or 7 nodes (respectively for 8-cell-stage blastomeres and 16-cell-stage blastomeres doublets) are then taken to fit a circle and compute the local curvature from the inverse radius of this circle. Taking the local curvatures along the cell perimeter over time, a kymograph of local curvature is created. Applying a Fourier transform on the curvature changes over time at each node, we obtain the amplitude of nodes that are classified either as apical or non-apical, based on the mTmG signal that is enriched on the apical domain excluding about 10 nodes around the transition between apical to non-apical domains. For doublets, nodes are classified either as inner or outer cell, based on, when applicable, the asymmetry of the internal contact angles (the cell with the largest internal contact angle being designated as the inner cell for ratio calculation) and/or, when applicable, by the asymmetry in cell size (the smallest cell being designated as the inner cell for ratio calculation). About 10 nodes near the contact edges are excluded from the analysis.

Code availability. Codes are available upon request.

Statistics. Mean, standard deviation, correlation coefficient, two-tailed Student's *t*-test and single-tailed Mann–Whitney *U*-test *P* values are calculated using Excel (Microsoft). Statistical significance of correlation coefficients is obtained from the Pearson correlation table.

The sample size was not predetermined and simply results from the repetition of experiments. No sample was excluded. No randomization method was used. The investigators were not blinded during experiments.

29. Riedl, J. *et al.* Lifeact mice for studying F-actin dynamics. *Nature Methods* **7,** 168–169 (2010).
30. Muzumdar, M. D., Tasic, B., Miyamichi, K., Li, L. & Luo, L. A global double-fluorescent Cre reporter mouse. *Genesis* **45,** 593–605 (2007).
31. Balbach, S. T. *et al.* Nuclear reprogramming: kinetics of cell cycle and metabolic progression as determinants of success. *PLoS ONE* **7,** e35322 (2012).
32. de Vries, W. N. *et al.* Expression of Cre recombinase in mouse oocytes: a means to study maternal effect genes. *Genesis* **26,** 110–112 (2000).
33. Ma, X. *et al.* Conditional ablation of nonmuscle myosin II-B delineates heart defects in adult mice. *Circ. Res.* **105,** 1102–1109 (2009).
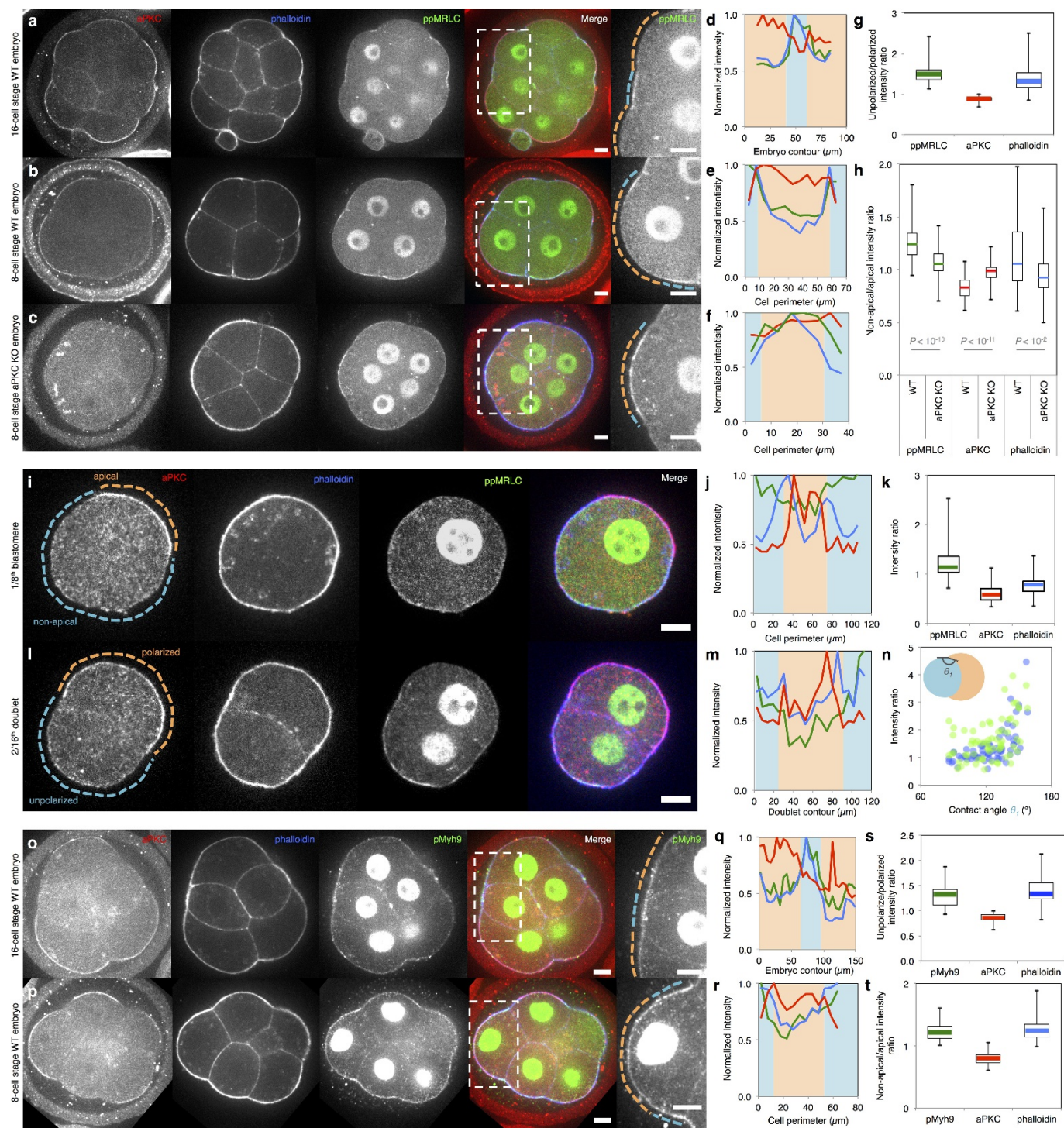
Extended Data Figure 1 | See next page for caption.
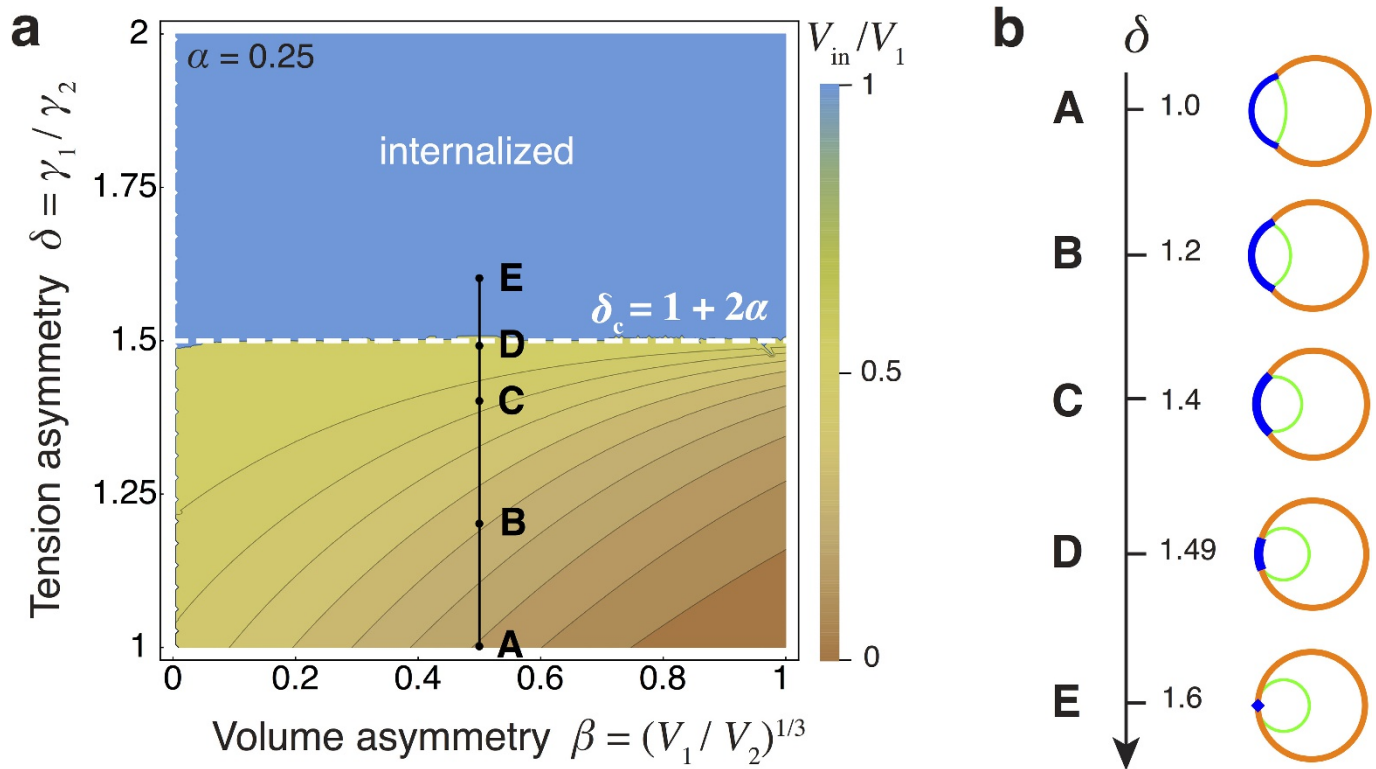
Extended Data Figure 1 | aPKC antagonizes myosin phosphorylation at the apical domain. a–c, Immunostaining of 16- (a) and 8-cell-stage wild-type (b) and aPKC-knockout (c) embryos showing aPKC (red), phalloidin (blue) and bi-phosphorylated myosin regulatory light chain (ppMRLC; green). Enlarged images of ppMRLC are shown on the far right. d–f, Cortical intensity profiles under the dotted lines in the far right panels of a–c. Apical domains are highlighted in orange and non-apical regions in blue. g, h, Box plot of unpolarized/polarized blastomere intensity ratio at the 16-cell stage (43 neighbouring blastomeres from 35 embryos from 3 experiments) and non-apical/apical intensity ratio at the 8-cell stage for wild-type (WT) and aPKC-knockout (KO) embryos (68 and 58 blastomeres from 22 and 12 embryos from 2 and 3 experiments, respectively). ppMRLC is in green, aPKC in red and phalloidin in blue. Student's t-test P values between wild type and aPKC knockout. At the 16-cell stage (a, d, g), blastomeres showing accumulations of ppMRLC and phalloidin at their cell-medium interfaces have less aPKC. At the 8-cell stage, the apical domain does not occupy the entirety of the cell-medium interface (b, e). The aPKC-rich apical domain shows less myosin than the aPKC-poor region of the cortex (b, e, h). In aPKC-knockout embryos (c, f, h), no aPKC-rich, nor ppMRLC-poor regions can be observed at the cell-medium interface of blastomeres. i, Immunostaining of 8-cell-stage blastomeres showing aPKC (red), phalloidin (blue), ppMRLC (green) and merged staining. The apical domain is highlighted in orange, the non-apical cortex in blue. Scale bar, 10 μm. j, Intensity profile along the cell perimeter showing aPKC (red), phalloidin (blue) and ppMRLC (green). The apical intensity is highlighted in orange, the non-apical cortex in blue. k, Box plot of apical and non-apical intensity ratio of cortical aPKC (red), phalloidin (blue) and ppMRLC (green) for 27 blastomeres from 3 experiments. Blastomeres isolated at the 8-cell stage show an aPKC-rich region (i–k), which has less cortical ppMRLC and phalloidin than the aPKC-poor region of the cell-medium interface. The ppMRLC- and actin-rich regions are distinct from the basolateral domain of cells (their

cell–cell contact), which have less ppMRLC and actin (a–c, l)[12]. This ppMRLC cortical region is therefore labelled 'non-apical'. l, Immunostaining of doublets of 16-cell-stage blastomeres showing aPKC (red), phalloidin (blue), ppMRLC (green) and merged staining. The polarized blastomere is highlighted in orange, the unpolarized one in blue. Scale bar, 10 μm. m, Intensity profile along the doublet perimeter showing aPKC (red), phalloidin (blue) and ppMRLC (green). The polarized blastomere is highlighted in orange, the unpolarized one in blue. Blastomeres isolated at the 8-cell stage divide to give rise to doublets of 16-cell-stage blastomeres[2,16]. The polarized sister cell shows high aPKC and low ppMRCL/phalloidin at their cell-medium interfaces when compared to the non-polarized sister cell (l, m). n, Cortical intensity ratio of ppMRLC (green) and phalloidin (blue) between the inner and outer cells as a function of the inner contact angles θ_1 (Pearson $R = 0.464$ and 0.614, $n = 67$ doublets from 2 experiments, $P < 0.001$). During the 16-cell stage, polarized blastomeres can envelop their unpolarized sister blastomeres (Supplementary Video 5)[2,16]. As envelopment occurs, the internal contact angles change (Extended Data Fig. 2). As the internal contact angles change, the asymmetry in cortical ppMRLC and phalloidin between sister blastomeres changes. After another division, a cyst consisting of four blastomeres forms (Supplementary Video 5). This structure is equivalent to the blastocyst in terms of gene expression[16] (Fig. 4). o, p, Immunostaining of 16- (o) and 8-cell-stage (p) embryos showing aPKC (red), phalloidin (blue) and myosin heavy chain phosphorylated on S1943 (pMyh9; green). Enlarged images of ppMRLC are shown on the far right. q, r, Cortical intensity profiles under the dotted lines on the far right of o, p. Apical domains are highlighted in orange and non-apical regions in blue. s, t, Box plot of unpolarized/polarized blastomere intensity ratio at the 16-cell stage (24 neighbouring blastomeres from 16 embryos from 3 experiments) and non-apical/apical intensity ratio at the 8-cell stage (34 blastomeres from 10 embryos from 3 experiments). pMyh9 in green, aPKC in red and phalloidin in blue.
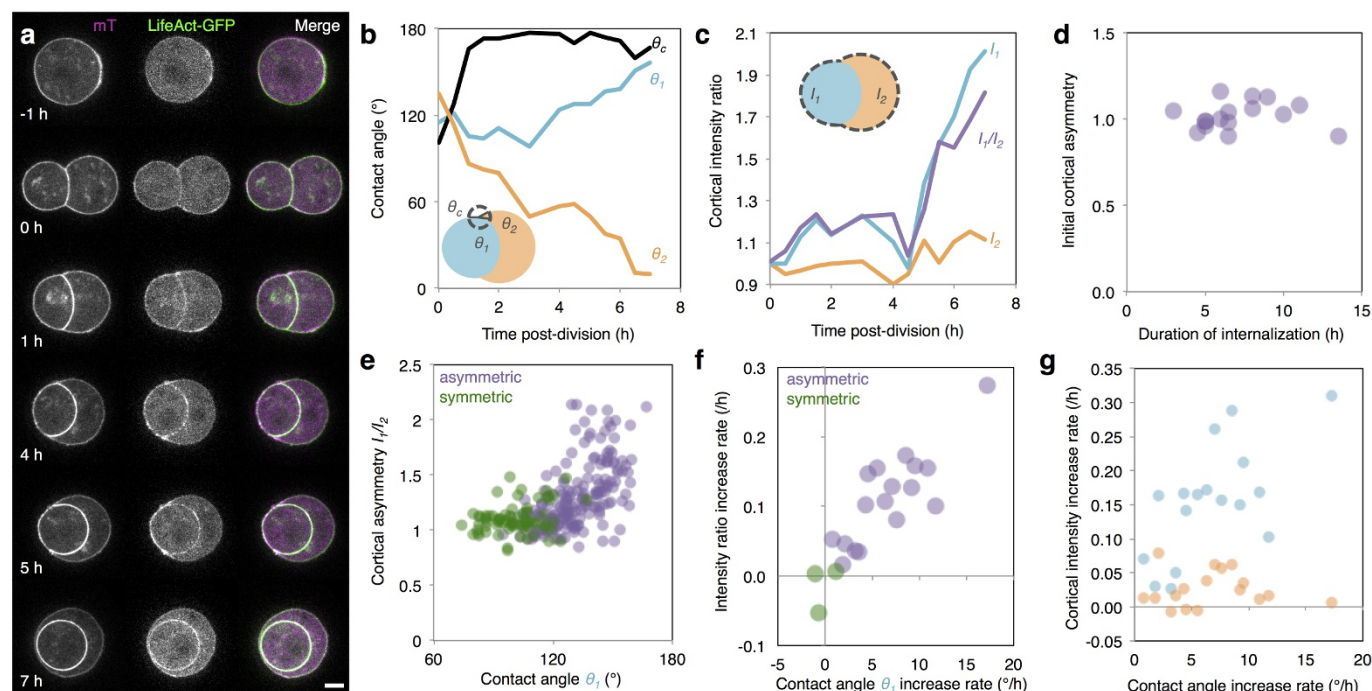
Extended Data Figure 2 | Cortical asymmetries intensify during the 16-cell stage. a, Time-lapse of mTmG (magenta) and LifeAct–GFP (green) expressing doublets of 16-cell-stage blastomeres. Scale bar, 10 μm. **b, c**, External (θ_c), and internal (θ_1 and θ_2) contact angles (**b**) and cortical LifeAct–GFP intensities of unpolarized I_1 and polarized I_2 blastomeres and intensity ratio I_1/I_2 (**c**) over time for the doublet shown in **a**. Blastomeres isolated at the 8-cell stage can divide asymmetrically to give rise to a polarized blastomere that will envelop its unpolarized sister blastomere (**a**). The external contact angle θ_c shows a rapid re-compaction of the cell doublet after division (**b**). The internal contact angles θ_1 and θ_2 indicate the progression of the envelopment process (**b**). As this happens, the cortical intensity of LifeAct–GFP of the internalizing blastomere I_1 increases while the one of the enveloping blastomere I_2 remains comparably more stable (**c**). This increases the cortical asymmetry I_1/I_2 (**c**). **d**, Initial cortical asymmetry over internalization time of doublets of 16-cell-stage blastomeres (Pearson $R = 0.064$, $n = 16$ doublets from 4 experiments, $P > 0.1$). The initial cortical asymmetry, calculated within 30 min after division, is 1.0 ± 0.1 (mean ± s.d., $n = 17$ doublets from 4 experiments) and does not control the time it takes for envelopment

to occur (**d**). **e**, Intensity ratio as a function of the contact angle θ_1 of doublets throughout the 16-cell-stage blastomeres (Pearson $R = 0.573$, 186 measurements on 17 asymmetric doublets (purple), $P < 0.001$ and Pearson $R = 0.266$, 69 measurements on 3 symmetric (green) doublets, $P < 0.1$, from 4 experiments). As the internal contact angles change, the asymmetry in cortical LifeAct–GFP between sister blastomeres with distinct polarity changes. **f**, Cortical intensity ratio increase rate as a function of the contact angle θ_1 increase rate (Pearson $R = 0.824$, $n = 17$ asymmetric (purple), $P < 0.001$, and Pearson $R = 0.393$, $n = 3$ symmetric (green) doublets, $P > 0.1$, from 4 experiments). **g**, Cortical intensity increase rate as a function of the contact angle increase rate for the polarized (orange, Pearson $R = -0.026$, $n = 17$ asymmetric doublets, $P > 0.1$) and unpolarized blastomere (blue, Pearson $R = 0.658$, $n = 17$ asymmetric doublets, $P < 0.01$) of a doublet resulting from asymmetric division or of two polarized cells resulting from a symmetric division (green, Pearson $R = -0.011$, $n = 3$ symmetric doublets, $P > 0.1$), from 4 experiments. The rates are correlated, which suggests that the dynamics of internalization and the dynamics of building up of cortical asymmetries are linked.

a

$\alpha = 0.25$

internalized

$\delta_c = 1 + 2\alpha$

V_{in}/V_1

Tension asymmetry $\delta = \gamma_1 / \gamma_2$

Volume asymmetry $\beta = (V_1 / V_2)^{1/3}$

E
D
C
B
A

b δ

A — 1.0
B — 1.2
C — 1.4
D — 1.49
E — 1.6

Extended Data Figure 3 | Cell size has no influence on internalization. Phase diagram describing the mechanical equilibrium of a cell within a doublet or embryo as function of the cell size asymmetry parameter β and the tension asymmetry parameter δ, for a fixed compaction parameter $\alpha = 0.25$. The colour code measures the degree of internalization, defined as the proportion of internalized volume V_{in}/V_1, which equals 1 for the internalized cell. The dotted line indicates the threshold value δ_c at which internalization occurs. An example of internalization with $\beta = 0.5$ is indicated in black (from A to E). Changing the volume asymmetry does not change the internalization threshold. Internalization of a doublet with $\beta = 0.5$ obtained with the analytical model for the same values of δ as indicated in the diagram from A to E.
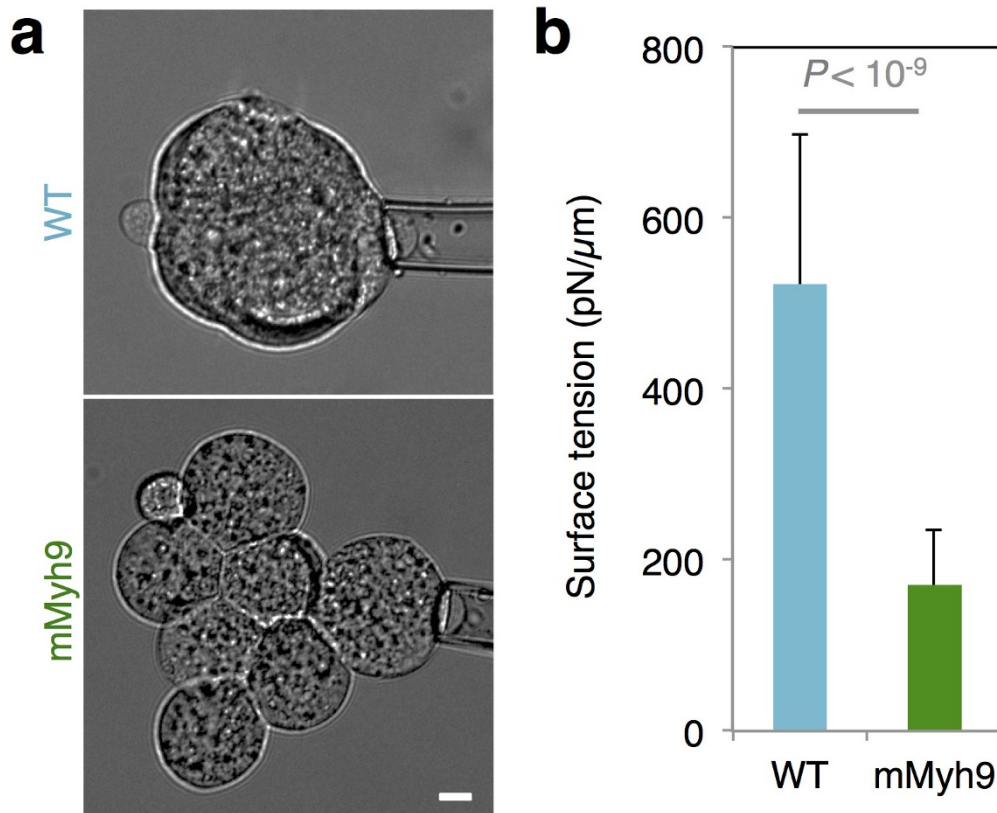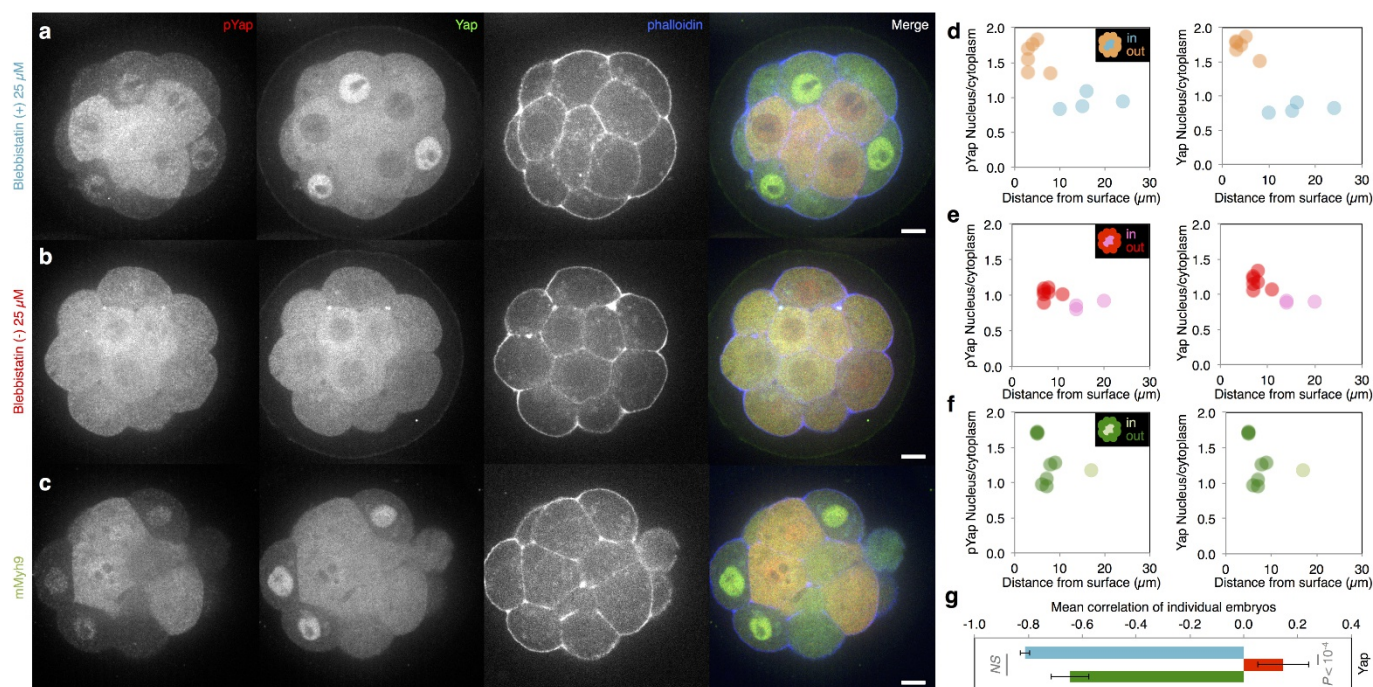
Extended Data Figure 4 | Contractility is required for internalization. Brightfield images of tension measurement on wild-type (WT; top) and mMyh9 (bottom) 8-cell-stage embryos. Scale bar, 10 μm. Mean ± s.d. of 25 blastomeres from 4 wild-type embryos and 26 blastomeres from 7 mMyh9 embryos from 2 experiments, Student's t-test $P < 10^{-9}$.
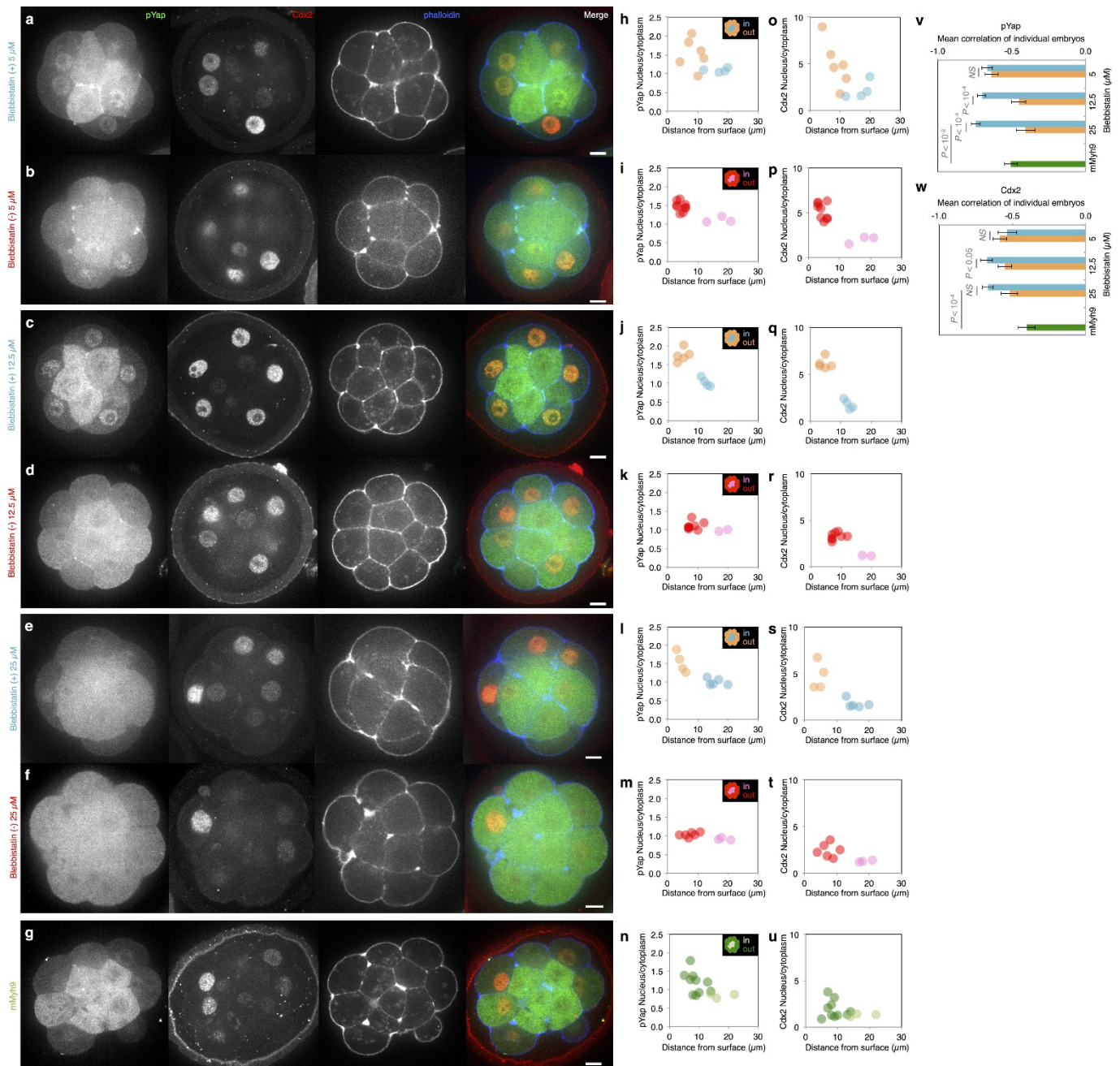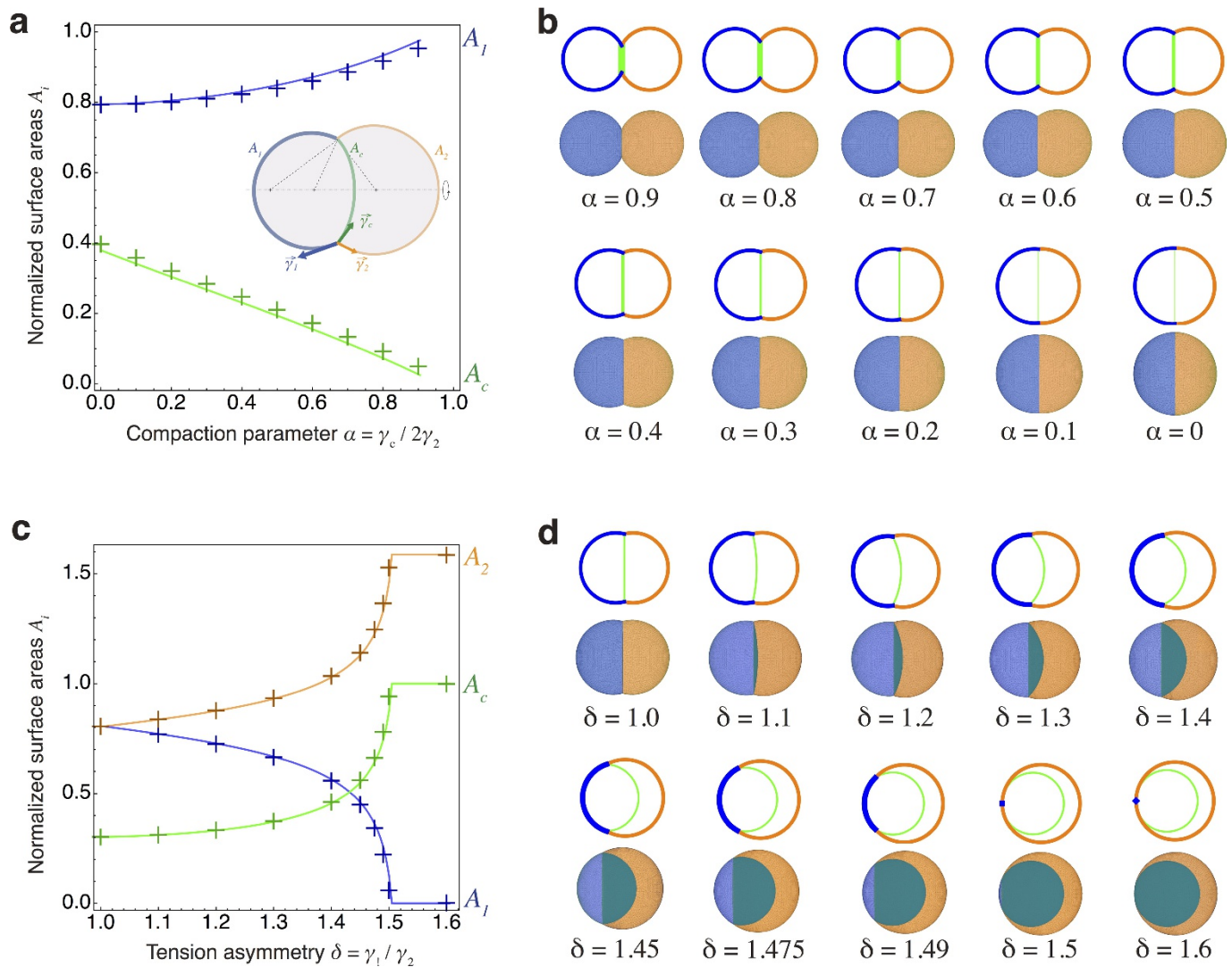
Extended Data Figure 5 | Control of pYap and Cdx2 localization by contractility in a dose-dependent manner. a–g, Immunostaining of wild-type embryos treated for 3 h with Bb(+) at 5 (**a**), 12.5 (**c**) or 25 (**e**) μM or with Bb(−) at 5 (**b**), 12.5 (**d**) or 25 (**f**) μM or of mMyh9 embryos (**g**) showing pYap (green), Cdx2 (red) and phalloidin (blue). **h–u**, Nucleus-to-cytoplasm intensity ratio of pYap (**h–n**) or Cdx2 (**o–u**) as a function of the distance from the surface for wild-type embryo treated with Bb(+) (outer cells in orange and inner cells in blue) at 5 (**h, o**, corresponding embryo shown in **a**), 12.5 (**j, q**, corresponding embryo shown in **c**) or 25 (**l, s**, corresponding embryo shown in **e**) μM or with Bb(−) (outer cells in red and inner cells in pink) at 5 (**i, p**, corresponding embryo shown in **b**), 12.5 (**k, r**, corresponding embryo shown in **d**) or 25 (**m, t**, corresponding embryo shown in **f**) μM and for mMyh9 embryos (**n, u**, corresponding embryo shown in **g**). **v, w**, Mean ± s.e.m. Pearson correlation values between the nucleus to cytoplasm intensity ratio of pYap (**v**) or Cdx2 (**w**) as a function of the distance from the surface from individual embryos. Two-hundred and seven blastomeres from 20 embryos for Bb(+) 5 μM, 252 blastomeres from 29 embryos for Bb(+) 12.5 μM, 179 blastomeres from 18 embryos for Bb(−) 5 μM and 267 blastomeres from 28 embryos for Bb(−) 12.5 μM from 3 experiments each. Two-hundred and eighty-one cells from 28 embryos from 5 experiments for pYap and 136 cells from 13 embryos from 4 experiments for Cdx2 for 25 μM Bb(+), 241 cells from 32 embryos from 5 experiments for pYap and 192 cells from 22 embryos from 4 experiments for Cdx2 for 25 μM Bb(−), and 349 cells from 32 embryos from 6 experiments for pYap and 217 cells from 21 embryos from 3 experiments for Cdx2 for mMyh9. Student's *t*-test *P* values; NS, not significant.

Extended Data Figure 6 | Contractility controls Yap subcellular localization. a–c, Immunostaining of wild-type embryos treated with 25 μM Bb(+) (**a**; an inactive enantiomere of the inhibitor) or Bb(−) (**b**; the selective inhibitor of myosin II ATPase activity) for 3 h or mMyh9 embryos (**c**) showing Yap (green), pYap (red) and phalloidin (blue). **d–f,** Nucleus-to-cytoplasm intensity ratio of pYap (left) and Yap (right) as a function of the distance from the surface for wild-type embryo treated with 25 μM Bb(+) (**d**; outer cells in orange and inner cells in blue, corresponding embryo shown in **a**) or Bb(−) (**e**; outer cells in magenta and inner cells in red, corresponding embryo shown in **b**) or mMyh9 embryo (**f**; outer cells in dark green and inner cells in light green, corresponding embryo shown in **c**). **g,** Mean ± s.e.m. Pearson correlation values between the nucleus to cytoplasm intensity ratio of Yap as a function of the distance from the surface from individual embryos. Two-hundred and fifty-two cells from 29 embryos for Bb(+), 201 cells from 26 embryos for Bb(−) and 132 cells from 12 embryos for mMyh9 from 3 experiments each. Student's *t*-test *P* value is shown; NS, not significant.

a, Normalized surface areas A_i vs Compaction parameter $\alpha = \gamma_c / 2\gamma_2$

b, Configurations at $\alpha = 0.9$, $\alpha = 0.8$, $\alpha = 0.7$, $\alpha = 0.6$, $\alpha = 0.5$, $\alpha = 0.4$, $\alpha = 0.3$, $\alpha = 0.2$, $\alpha = 0.1$, $\alpha = 0$

c, Normalized surface areas A_i vs Tension asymmetry $\delta = \gamma_1 / \gamma_2$

d, Configurations at $\delta = 1.0$, $\delta = 1.1$, $\delta = 1.2$, $\delta = 1.3$, $\delta = 1.4$, $\delta = 1.45$, $\delta = 1.475$, $\delta = 1.49$, $\delta = 1.5$, $\delta = 1.6$

Extended Data Figure 7 | Quantitative comparison between analytical and numerical results. a, Comparison of the surface areas of the cell medium (blue) and cell–cell interfaces (green) between the simulations (crosses) and the analytical model (lines) for different values of the compaction parameter α between 0 and 1. A schematic diagram of a cell doublet defining the cell medium and cell–cell surface tensions γ_1, γ_2 and γ_c and areas A_1, A_2 and A_c are shown as an inset. **b**, Configurations of doublets as predicted by the analytical model and simulations for the

discrete values of α corresponding to the plot in **a**. **c**, Comparison of the surface areas of the cell-medium interfaces of cell 1 (blue), 2 (orange) and of the cell–cell interface (green) between the simulations (crosses) and the analytical model (lines) for different values of the tension asymmetry parameter δ between 1 and 1.6 fixed compaction parameter $\alpha = 0.25$. **d**, Configurations of doublets as predicted by the analytical model and simulations for the discrete values of δ corresponding to the plot in **c**.